



*Supplement of*

## **Lasting impact of winds on Arctic sea ice through the ocean's memory**

**Qiang Wang et al.**

*Correspondence to:* Qiang Wang ([qiang.wang@awi.de](mailto:qiang.wang@awi.de))

The copyright of individual parts of the supplement might differ from the article licence.

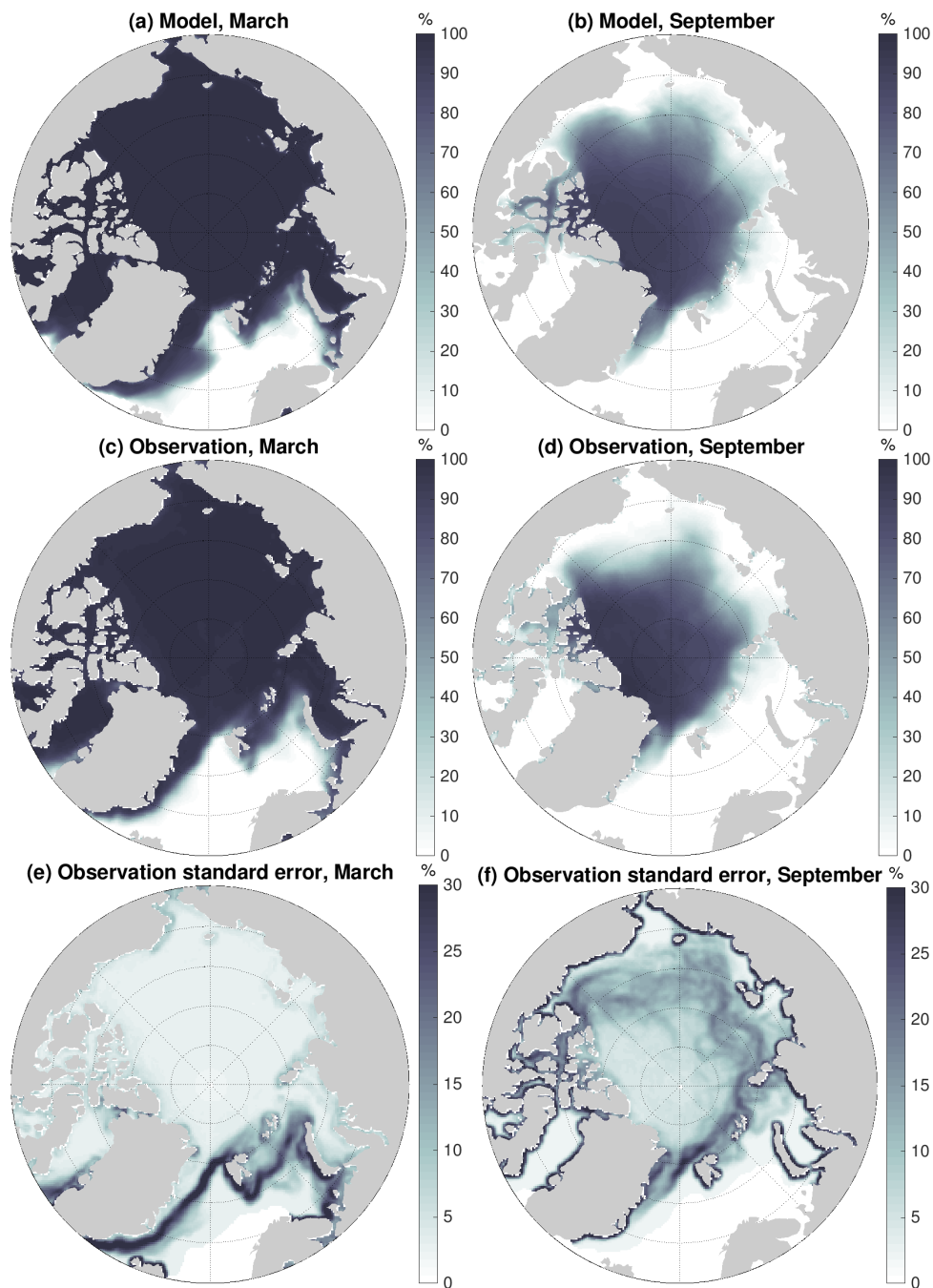


**Figure S1.** (upper) Simulated sea ice concentration in (a) March and (b) September. (middle) OSI-SAF observed sea ice concentration in (c) March and (d) September. The average over 2000-2019 is shown. The observational uncertainty is shown in (e) for March and (f) for September. Observation reference: Lavergne, T., Sørensen, A. M., Kern, S., Tonboe, R., Notz, D., Aaboe, S., Bell, L., Dybkjær, G., Eastwood, S., Gabarro, C., Heygster, G., Killie, M. A., Brandt Kreiner, M., Lavelle, J., Saldo, R., Sandven, S., and Pedersen, L. T.: Version 2 of the EUMETSAT OSI SAF and ESA CCI sea-ice concentration climate data records, *The Cryosphere*, 13, 49-78, 2019.

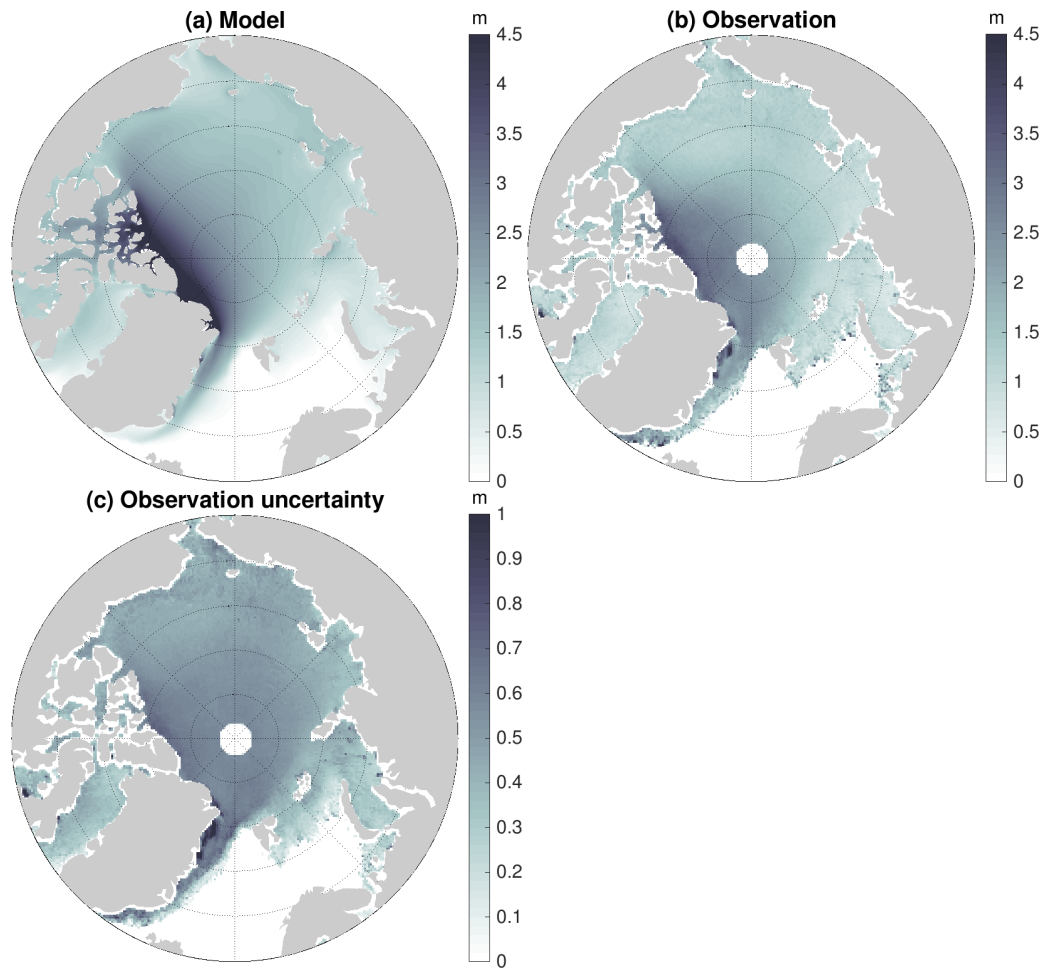


**Figure S2.** (a) Simulated and (b) CryoSat-2 observed sea ice thickness averaged over months with observations available (October to April) from 2011 to 2019. (c) The CryoSat-2 observation uncertainty. Observation reference: Hendricks, S. and Ricker, R. (2019): Product User Guide Algorithm Specification: AWI CryoSat-2 Sea Ice Thickness (version 2.2).

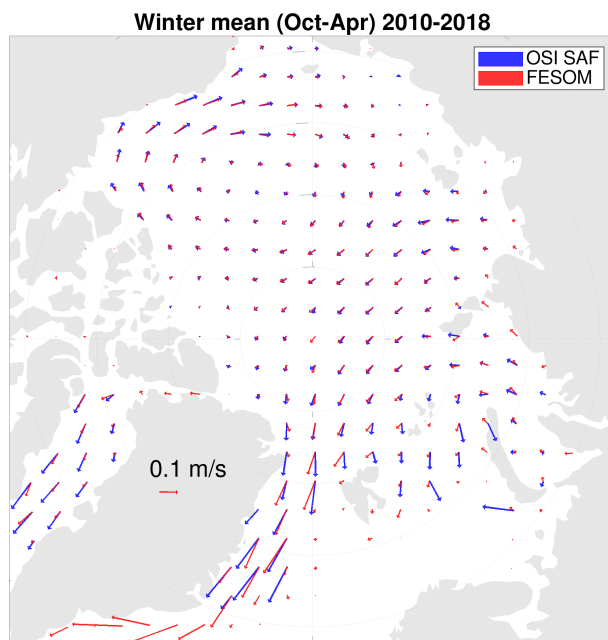


**Figure S3.** Sea ice drift in the OSI-SAF observation (Lavergne et al., 2010) and control model simulation. The average is taken over cold seasons (October to April) in the period of 2010-2018. The same scaling is used for the arrows of both the observation and model. Reference: Lavergne, T., Eastwood, S., Teffah, Z., Schyberg, H. and L.-A. Breivik (2010), Sea ice motion from low resolution satellite sensors: an alternative method and its validation in the Arctic. *J. Geophys. Res.*, 115, C10032, doi:10.1029/2009JC005958

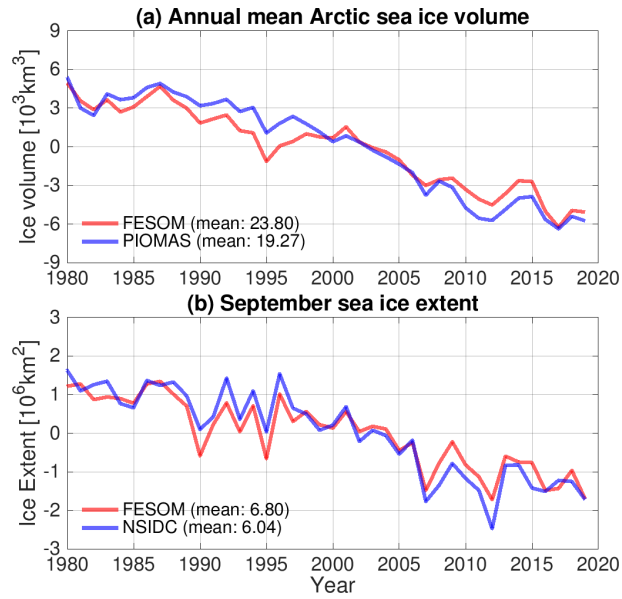


**Figure S4.** (a) Arctic annual mean sea ice volume from the control run and the Pan-Arctic Ice Ocean Modeling and Assimilation System (PIOMAS) result (Schweiger et al., 2011). (b) Arctic September sea ice extent from the control run and the National Snow and Ice Data Center (NSIDC) satellite observation (Fetterer et al., 2017). The anomalies are relative to the respective mean values, and the mean values are shown in the legends.

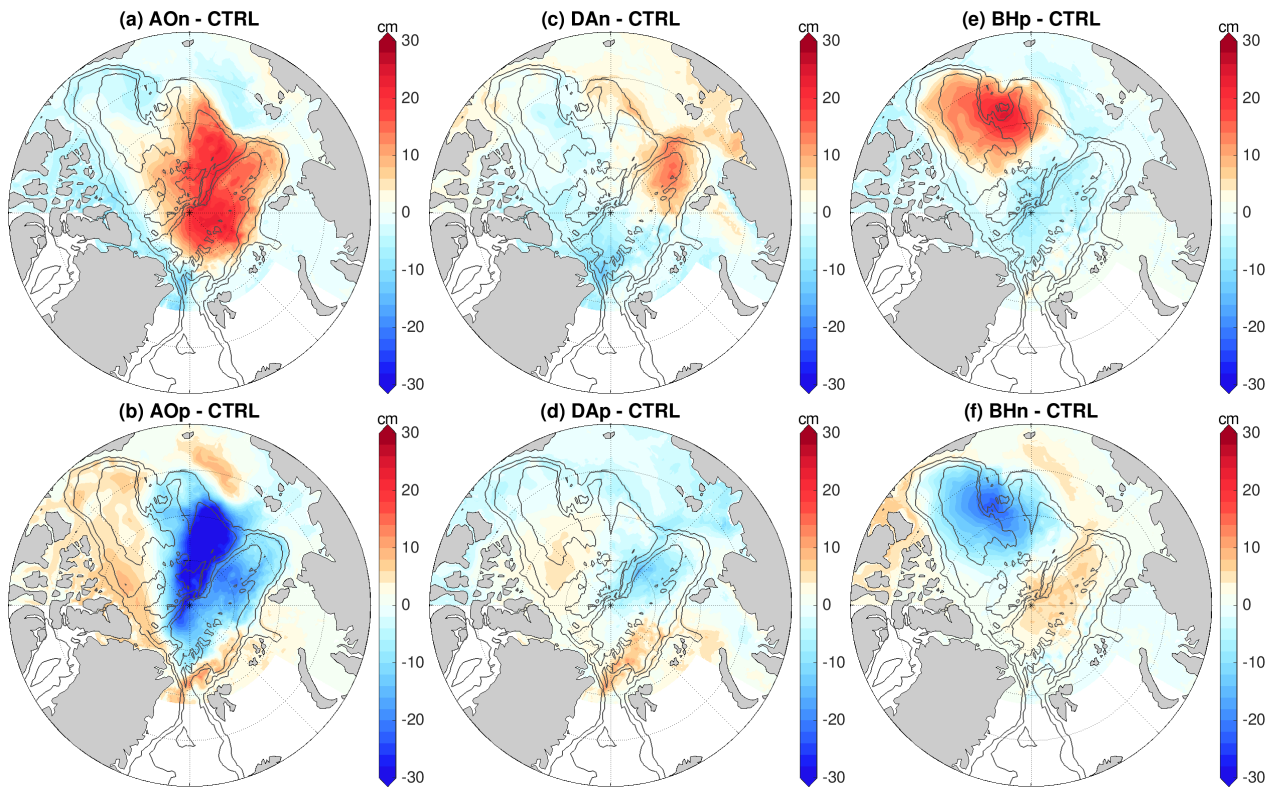


**Figure S5.** Anomaly of halosteric height (cm) relative to the control run in the sixth year (2015) of the wind-perturbation simulations: (a) negative phase of Arctic Oscillation (AO) forcing, (b) positive phase of AO forcing, (c) negative phase of Dipole Anomaly (DA) forcing, (d) positive phase of DA forcing, (e) positive phase of Beaufort High (BH) forcing, and (f) negative phase of BH forcing. The halosteric height is referenced to 400 m depth or the ocean bottom if it is shallower than 400 m. The gray contour lines indicate the 500-, 2000- and 3500-m isobaths.

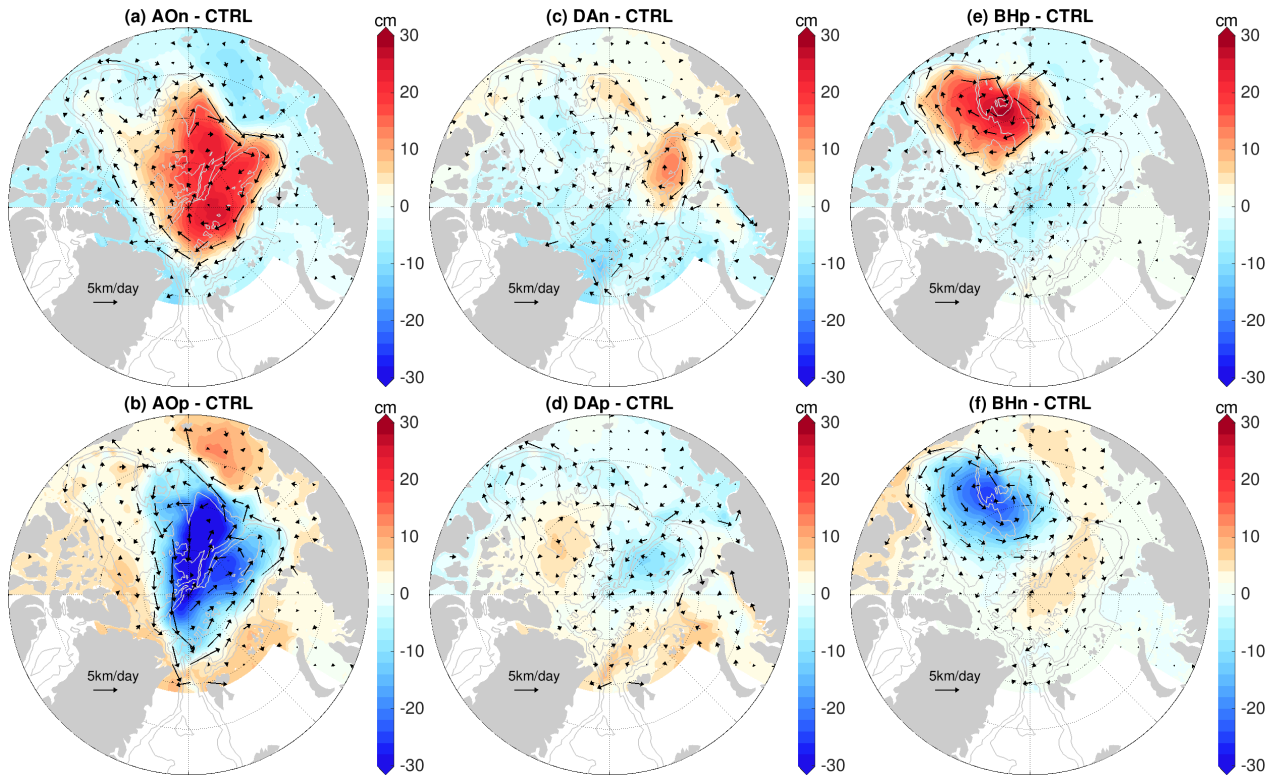


**Figure S6.** Anomaly of sea surface height (SSH, patch color) and surface geostrophic current (arrows) relative to the control run in the sixth year (2015) of the wind-perturbation simulations: (a) negative phase of Arctic Oscillation (AO) forcing, (b) positive phase of AO forcing, (c) negative phase of Dipole Anomaly (DA) forcing, (d) positive phase of DA forcing, (e) positive phase of Beaufort High (BH) forcing, and (f) negative phase of BH forcing. The gray contour lines indicate the 500-, 2000- and 3500-m isobaths.

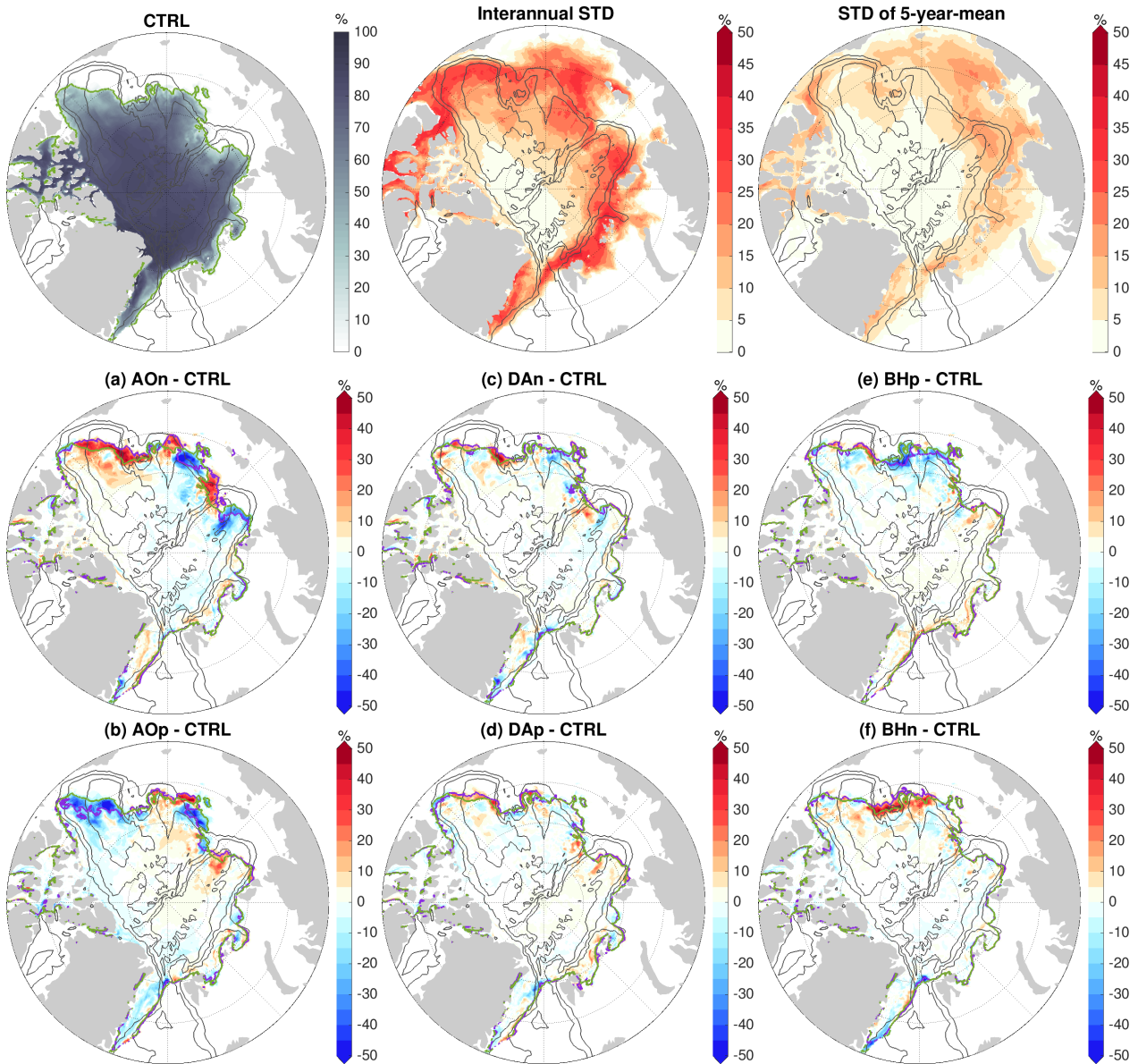


**Figure S7.** (a)-(f) September sea ice concentration anomaly *in the last year (2019)* of the sensitivity simulations in which wind perturbations were switched off: Experiments with an initial ocean spun up with (a) negative phase of Arctic Oscillation (AO) forcing, (b) positive phase of AO forcing, (c) negative phase of Dipole Anomaly (DA) forcing, (d) positive phase of DA forcing, (e) positive phase of Beaufort High (BH) forcing, and (f) negative phase of BH forcing. The anomaly is referenced to the control run. The September sea ice concentration in this year (left), the standard deviation (STD) of September sea ice concentration on the interannual time scale in the 2010s (middle), and the STD of pentadal mean in the period 1980-2019 (right) from the control run are shown on top of the figure for reference. The locations of sea ice edge (15% sea ice concentration) are indicated with green lines for the control run and violet lines for the sensitivity runs. The black contour lines indicate the 500-, 2000- and 3500-m isobaths.

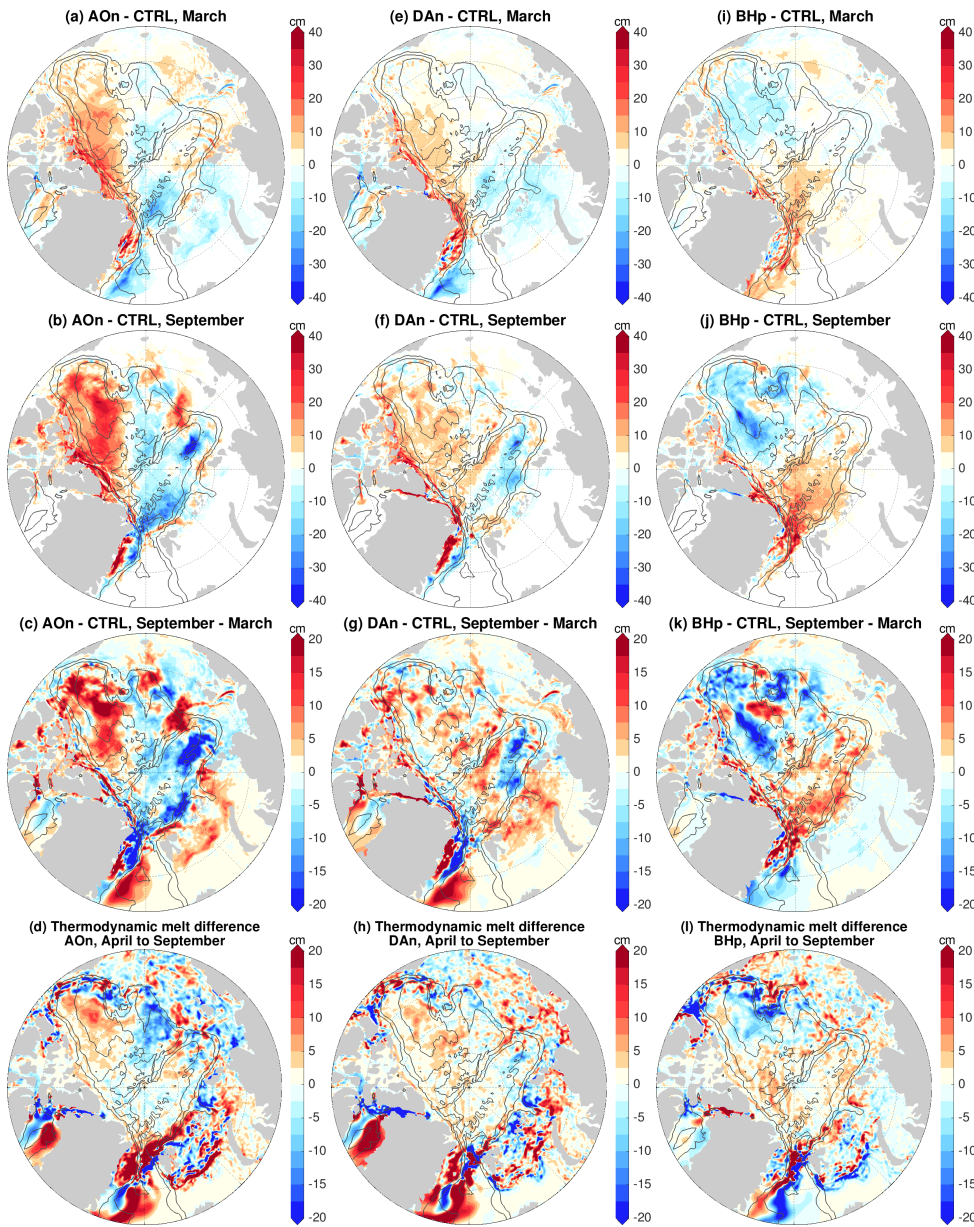


**Figure S8.** (a) Anomaly of March sea ice thickness averaged over the four model years in the experiment with an initial ocean spun up with the negative phase of Arctic Oscillation (AO) perturbation. (b) The same as (a), but for September sea ice thickness. (c) The difference between (a) and (b) (September minus March). (d) Anomaly of the change in sea ice thickness from March to September due to thermodynamics in the experiment with an initial ocean spun up with the negative phase of AO perturbation. The anomalies are relative to the control run. (e)(f)(g)(h) The same as (a)(b)(c)(d), but for the experiment with an initial ocean spun up with the negative phase of Dipole Anomaly (DA) perturbation. (i)(j)(k)(l) The same as (a)(b)(c)(d), but for the experiment with an initial ocean spun up with the positive phase of Beaufort High (BH) perturbation. The black contour lines indicate the 500-, 2000- and 3500-m isobaths. This figure indicates that the seasonal variations of sea ice thickness anomalies are mainly due to the direct effect of sea ice dynamics, although sea ice thermodynamics have some contribution. Note that the anomalies in sea ice thermodynamics are associated with the anomalies in sea ice drift, thus having a dynamics origin.

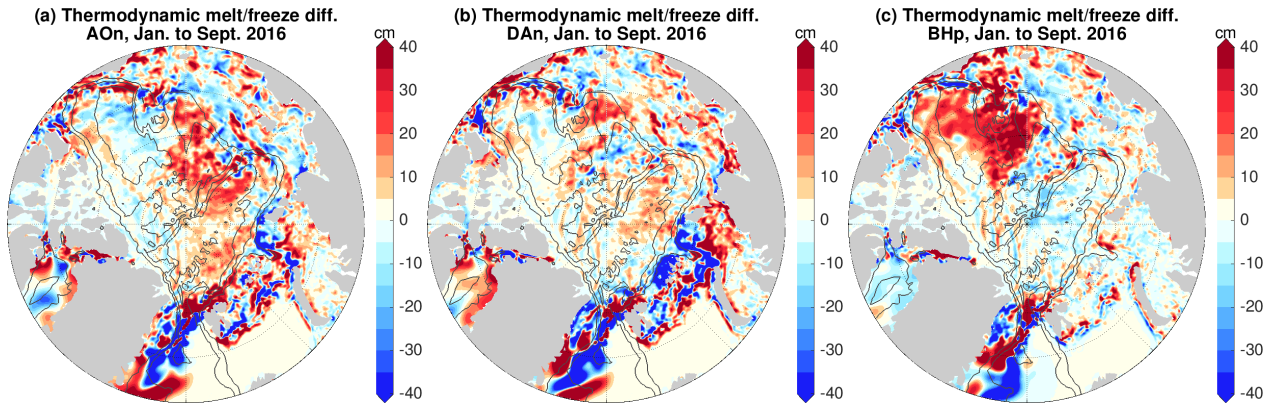


**Figure S9.** (a) Anomaly of the change in sea ice thickness from January to September in 2016 due to sea ice thermodynamics in the experiment with an initial ocean spun up with the negative phase of Arctic Oscillation (AO) perturbation *and with the sea surface height (SSH) gradient term in the momentum equation taken from the control run*. The anomalies are referenced to the control run. (b) The same as (a), but for the experiment with an initial ocean spun up with the negative phase of Dipole Anomaly (DA) perturbation; (c) The same as (a), but for the experiment with initial ocean spun up with the positive phase of Beaufort High (BH) perturbation. The black contour lines indicate the 500-, 2000- and 3500-m isobaths. Comparing this figure with Figure 10d-f in the main text reveals that the SSH gradient term in the sea ice momentum equation can significantly influence sea ice thermodynamics through influencing sea ice drift. Therefore, the anomalies of sea ice thermodynamics have a dynamical origin.

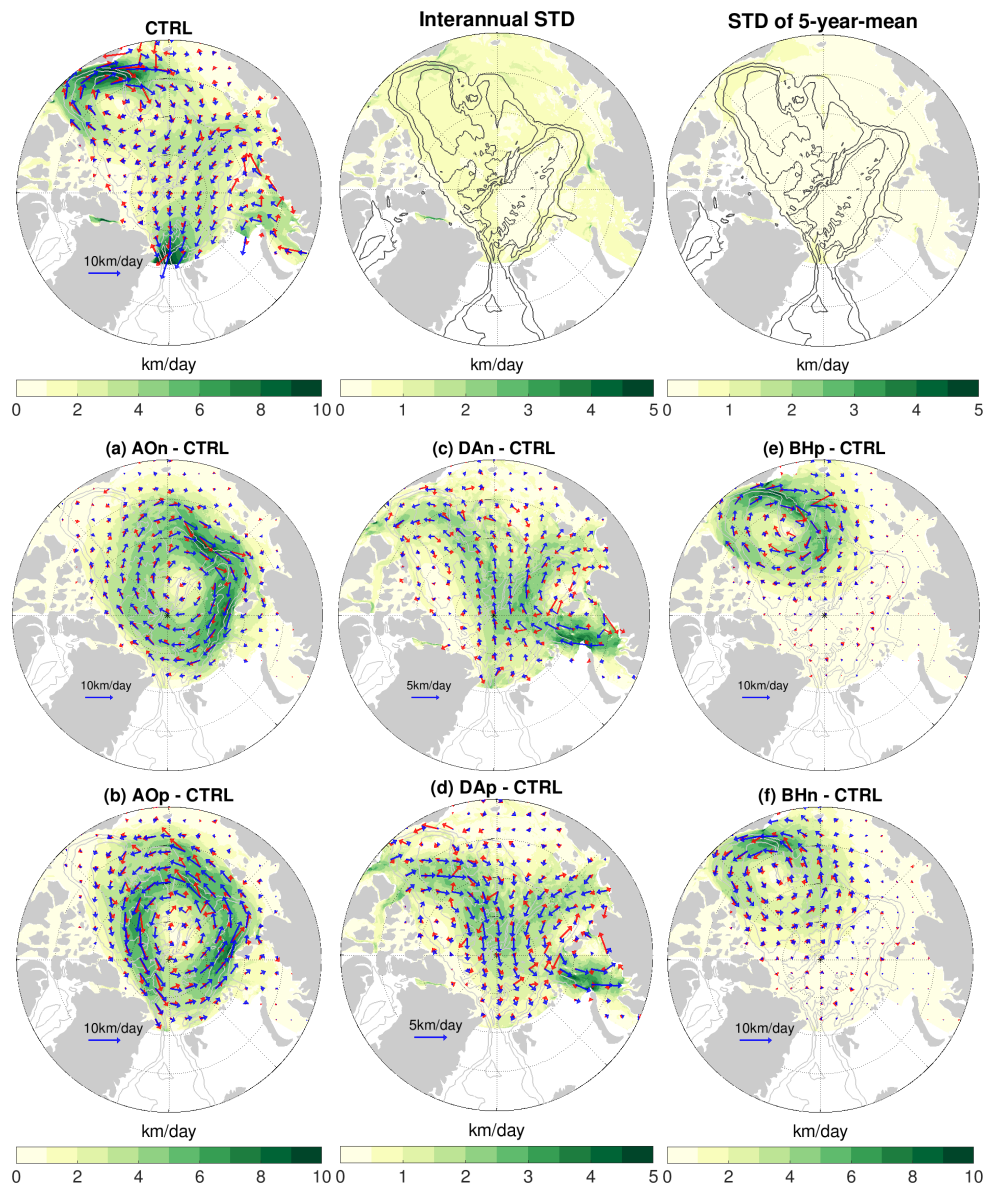


**Figure S10.** (a)-(f) Anomaly of sea ice drift (blue) and ocean surface geostrophic current (red) when wind perturbations were kept. Experiments with (a) negative phase of Arctic Oscillation (AO) forcing, (b) positive phase of AO forcing, (c) negative phase of Dipole Anomaly (DA) forcing, (d) positive phase of DA forcing, (e) positive phase of Beaufort High (BH) forcing, and (f) negative phase of BH forcing. The anomalies are averaged over 2016-2019 and referenced to the control run. The mean sea ice drift in this period (left), the standard deviation (STD) of sea ice drift speed on the interannual time scale in the 2010s (middle), and the STD of the pentadal mean in the period 1980-2019 (right) from the control run are shown on top of the figure for reference. The gray contour lines indicate the 500-, 2000- and 3500-m isobaths. *This figure shows the impacts of wind perturbations when they are present. It is to be compared with Figure 6 in the main paper that shows the impacts from the ocean's memory.*

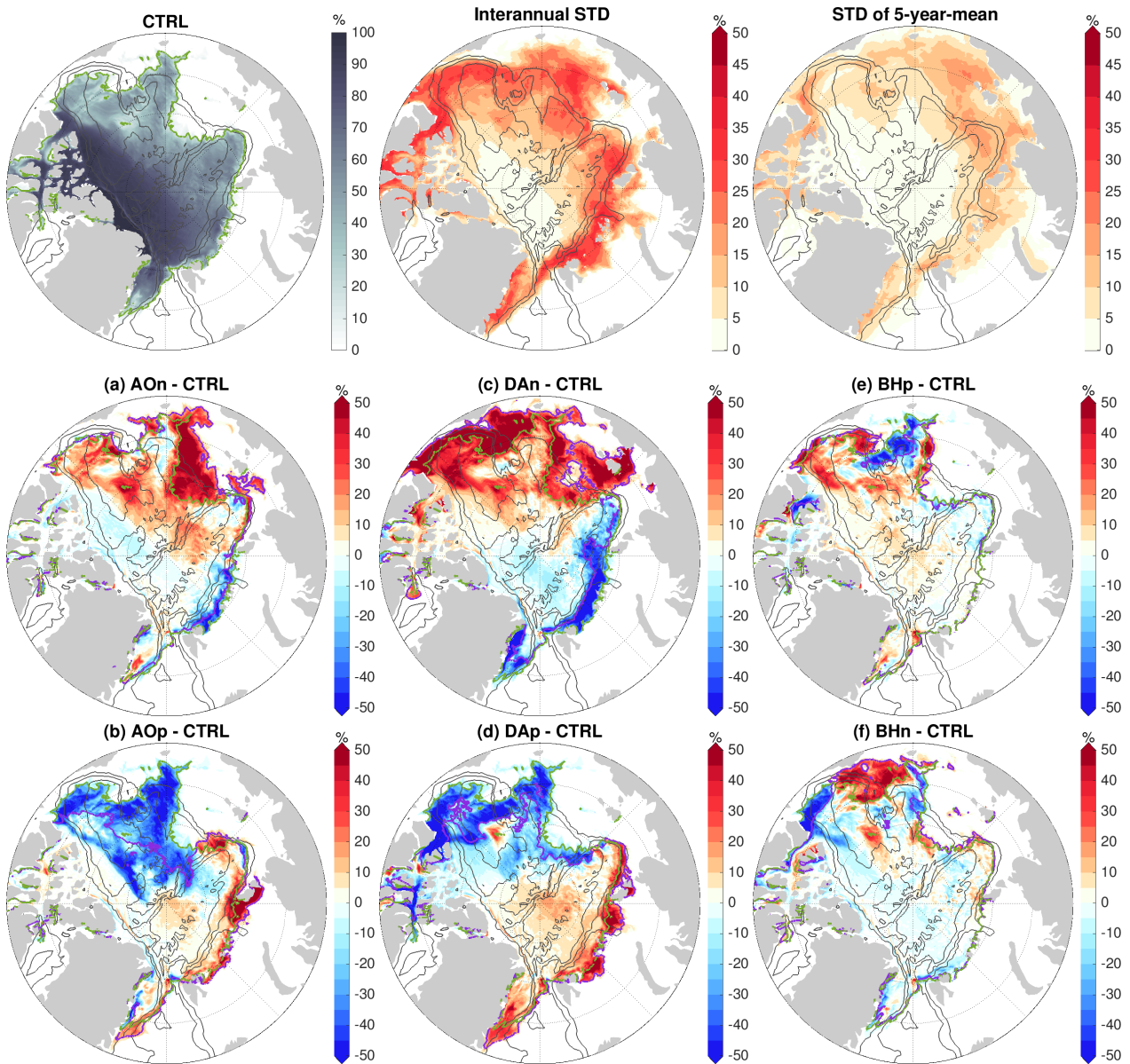


**Figure S11.** (a)-(f) September sea ice concentration anomaly in 2016 in the wind-perturbation simulations: Experiments with an initial ocean spun up with (a) negative phase of Arctic Oscillation (AO) forcing, (b) positive phase of AO forcing, (c) negative phase of Dipole Anomaly (DA) forcing, (d) positive phase of DA forcing, (e) positive phase of Beaufort High (BH) forcing, and (f) negative phase of BH forcing. The anomaly is referenced to the control run. The September sea ice concentration in this year (left), the standard deviation (STD) of September sea ice concentration on the interannual time scale in the 2010s (middle), and the STD of pentadal mean in the period 1980-2019 (right) from the control run are shown on top of the figure for reference. The locations of sea ice edge (15% sea ice concentration) are indicated with green lines for the control run and violet lines for the sensitivity runs. The black contour lines indicate the 500-, 2000- and 3500-m isobaths. *This figure shows the impacts of wind perturbations when they are present. It is to be compared with Figure 8 in the main paper that shows the impacts from the ocean's memory.*

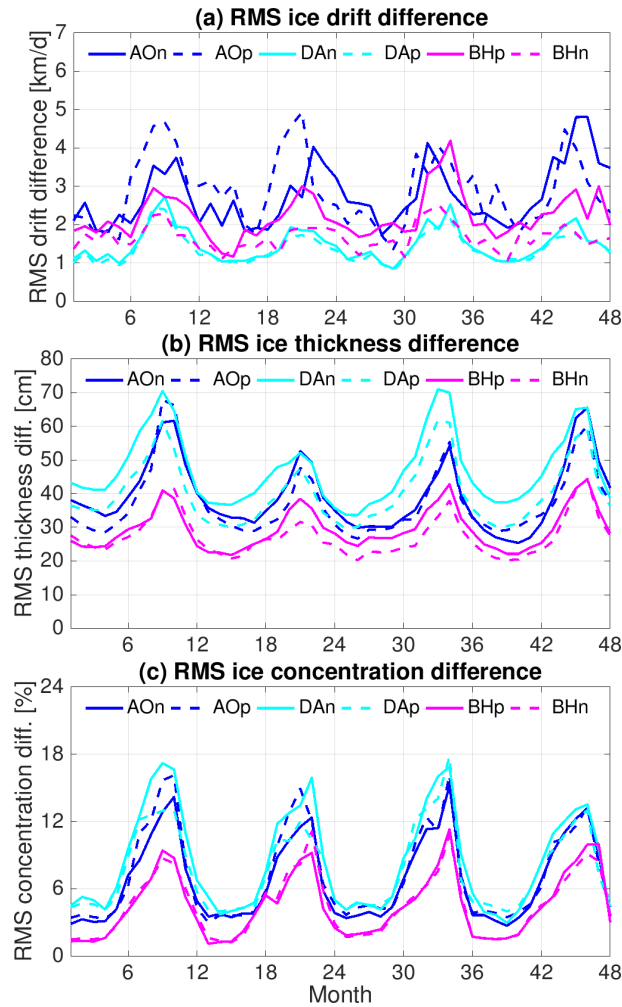


**Figure S12.** Monthly root-mean-square (RMS) difference of (a) sea ice drift, (b) thickness and (c) concentration between runs with wind perturbations and the control run. The RMS difference is calculated where sea ice concentration is larger than 20% in both simulations that are compared. *This figure shows the impacts of wind perturbations when they are present.* It is to be compared with Figure 9 in the main paper that shows the impacts from the ocean’s memory.

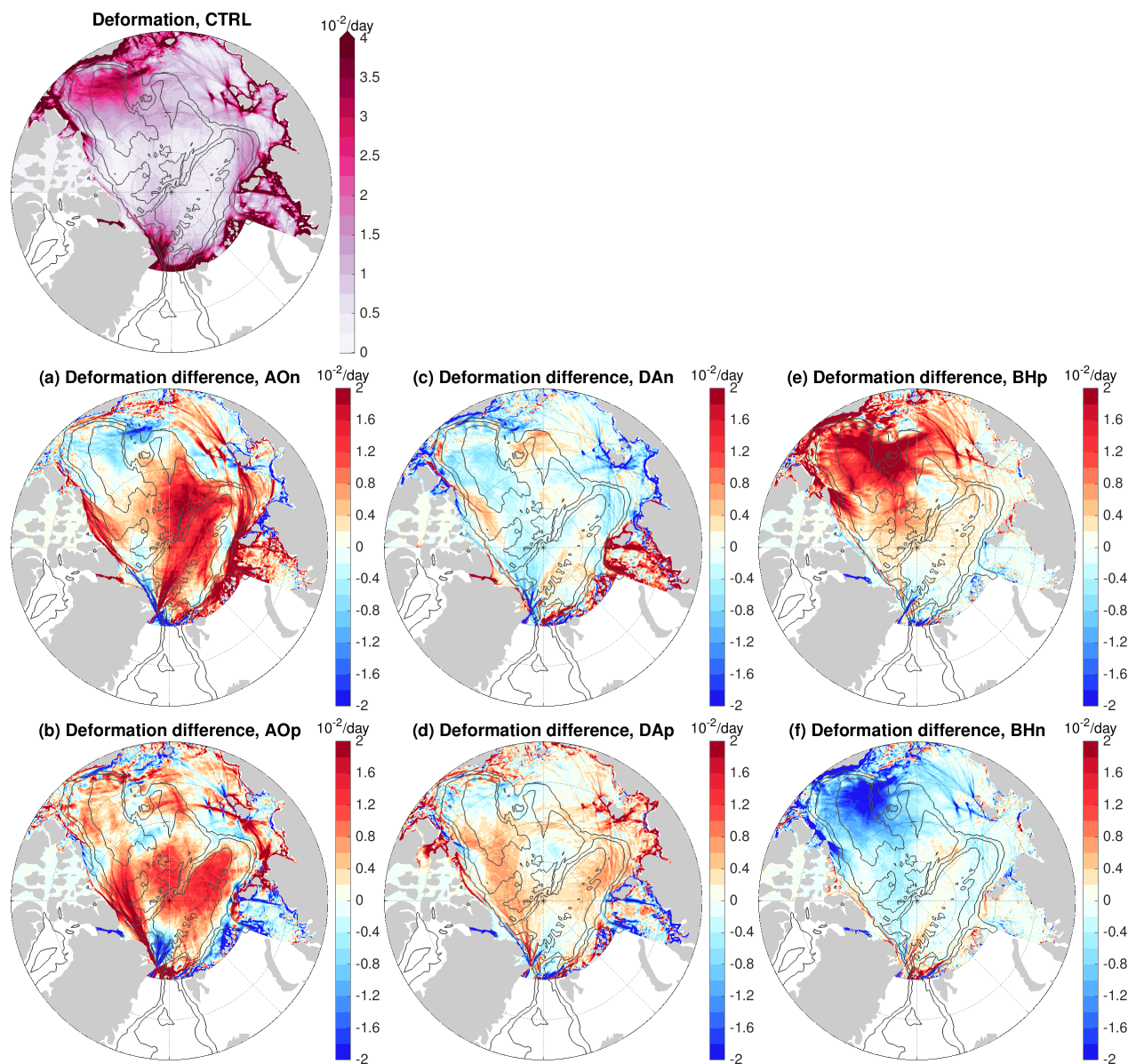


**Figure S13.** (a)-(f) Anomaly of sea ice deformation rate when wind perturbations were kept. Experiments with (a) negative phase of Arctic Oscillation (AO) forcing, (b) positive phase of AO forcing, (c) negative phase of Dipole Anomaly (DA) forcing, (d) positive phase of DA forcing, (e) positive phase of Beaufort High (BH) forcing, and (f) negative phase of BH forcing. The anomalies are averaged over 2016-2019 and referenced to the control run result, which is shown on top of the figure. *This figure shows the impacts of wind perturbations when they are present.* It is to be compared with Figure 13 in the main paper which shows the impacts from the ocean's memory.

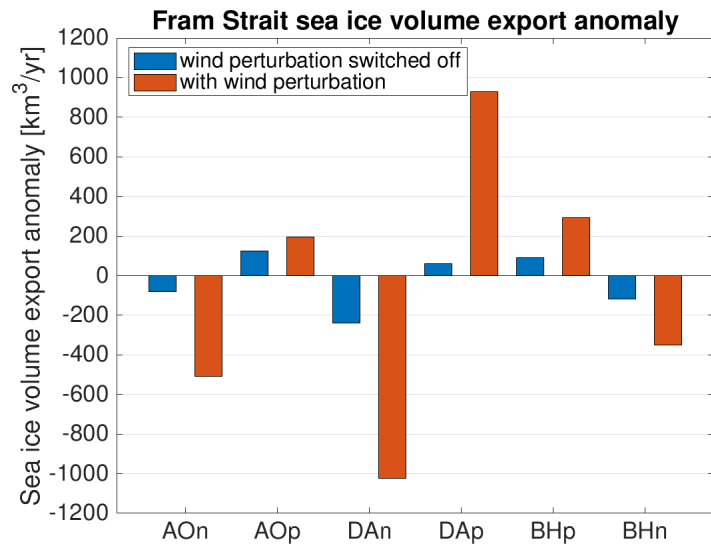


**Figure S14.** Anomaly of Fram Strait sea ice volume export in the sensitivity runs with wind perturbations switched off (blue) and in cases when the wind perturbations are kept (red). The anomalies are relative to the control run and averaged over 2016-2019. Positive values indicate larger export.